

Spatial Patterns, Mechanisms, and Predictability of Barents Sea Ice Change

ELINA EFSTATHIOU,^a TOR ELDEVIK,^a MARIUS ÅRTHUN,^a AND SIGRID LIND^b

^a *Geophysical Institute, University of Bergen, and Bjerknes Centre for Climate Research, Bergen, Norway*

^b *Norwegian Polar Institute, Tromsø, Norway*

(Manuscript received 16 January 2021, in final form 21 January 2022)

ABSTRACT: Recent Arctic winter sea ice loss has been most pronounced in the Barents Sea. Here we explore the spatial structure of Barents Sea ice change as observed over the last 40 years. The dominant mode of winter sea ice concentration interannual variability corresponds to areal change (explains 43% of spatial variance) and has a center of action in the northeastern Barents Sea where the temperate Atlantic inflow meets the wintertime sea ice. Sea ice area import and northerly wind also contribute to this “areal-change mode”; the area increases with more ice import and stronger winds from the north. The remaining 57% variance in sea ice, individually and combined, redistributes the sea ice without changing the total area. The two leading redistribution modes are a dipole of increase in sea ice concentration south of Svalbard with decrease southwest of Novaya Zemlya, and a tripole of increase in the central Barents Sea with decrease east of Svalbard and in the southeastern Barents Sea. Redistribution is mainly contributed by anomalous wind and sea ice area import. Basic predictability (i.e., the lagged response to observed drivers) is predominantly associated with the areal-change mode as influenced by temperature of the Atlantic inflow and sea ice import from the Arctic.

KEYWORDS: Arctic; Sea ice; Anomalies; Climate variability; Oceanic variability

1. Introduction


The Barents Sea (Fig. 1) is a hotspot of climate change. It has been warming faster than any other place in the Arctic (Screen and Simmonds 2013; Smedsrud et al. 2013; Lind et al. 2018) and has experienced the most pronounced winter sea ice loss (Onarheim et al. 2018; Årthun et al. 2021). In addition to the gradual retreat during recent decades, the Barents Sea ice cover displays pronounced interannual to decadal variability (Årthun et al. 2012), for example as evidenced by the relatively ice-rich winter 2019 equaling the mean extent for 1980–2019 (Fig. 1; Aaboe et al. 2021). This variability is also manifested as large fluctuations in the spatial distribution of the sea ice concentration, a spatial structure of change that remains largely unexplored. Sea ice coverage and its change are generally summarized and quantified as the time series of a single areal number, for the Arctic in general or when considering its individual regional seas (e.g., Kauker et al. 2003; Koenigk et al. 2009; Close et al. 2017; Onarheim et al. 2018; Årthun et al. 2021).

The retreat and variability in Barents Sea ice edge have to a large degree been ascribed to the variable inflow of Atlantic Water (AW) through the Barents Sea Opening (BSO; Fig. 1; Schlichtholz 2011; Årthun et al. 2012; Herbaut et al. 2015). Ocean temperature anomalies impacting the sea ice cover can also be generated or modified by local atmosphere–ocean interactions in the southern Barents Sea (Schlichtholz 2011; Bushuk et al. 2019; Skagseth et al. 2020).

Another source of variability is sea ice import to the Barents Sea from the Arctic Ocean (Ellingsen et al. 2009; Kwok 2009; Lind et al. 2018). This exchange takes place through two passages, a northern gateway between Svalbard and Franz Josef Land (NGW) and a more eastern gateway between Franz Josef Land and Novaya Zemlya (EGW; Fig. 1). The sea ice area import at these two gateways has a dual impact on the sea ice located in the Barents Sea: directly by adding or extracting ice, and indirectly by adding freshwater when melting, acting to increase ocean stratification and hence sustain conditions that are favorable for local sea ice growth (Rudels et al. 2004; Lind et al. 2018). The sea ice area import through the EGW is generally positive (i.e., inflow) and dominates the sea ice area inflow to the Barents Sea, whereas the NGW has a smaller and more variable sea ice area transport (Lind et al. 2018).

Atmospheric circulation is a main driver of sea ice motion (Wu et al. 2006; Wu and Johnson 2007; Kwok 2009; Kwok et al. 2013). The Arctic sea ice is becoming younger and thinner and thus drifts faster (Spren et al. 2011; Carmack et al. 2015). The drift includes sea ice inflows to the Barents Sea (Kwok et al. 2005; Kwok 2009; Lind et al. 2018). Local winds also contribute by redistributing sea ice within the Barents Sea (Pavlova et al. 2014) and by impacting local air–ice–ocean heat fluxes and accordingly impacting the local freezing and melting of sea ice (Sorokina et al. 2016; Woods and Caballero 2016). Northerly winds are for example well known to contribute to sea ice import from the Arctic and to distribute sea ice farther into the Barents Sea, thus extending the sea ice cover (Kwok et al. 2005).

The Barents Sea hosts some of Norway and Russia’s main fisheries and is generally a focal point of the increased

 Denotes content that is immediately available upon publication as open access.

Corresponding author: Elina Efstathiou, evangelia.efstathiou@uib.no



This article is licensed under a [Creative Commons Attribution 4.0 license](http://creativecommons.org/licenses/by/4.0/) (<http://creativecommons.org/licenses/by/4.0/>).

DOI: 10.1175/JCLI-D-21-0044.1

© 2022 American Meteorological Society.

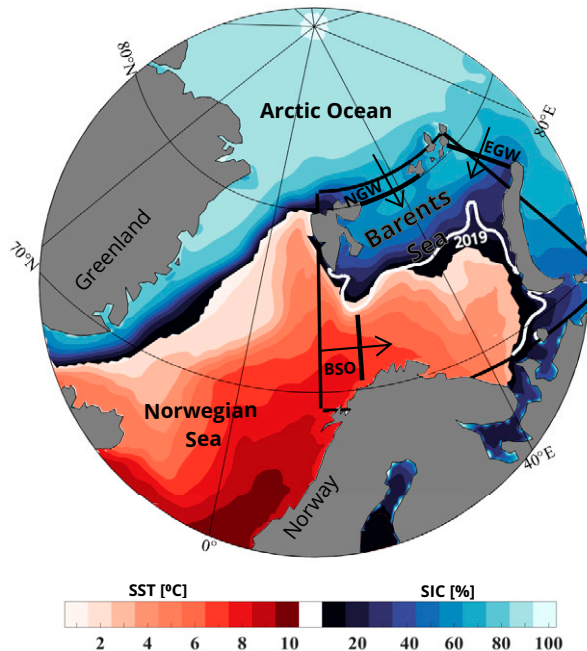


FIG. 1. The Barents Sea regional and climatological setting. The Barents Sea study region is contained within 13° – 63° E, 69° – 81° N (outlined in black). Red colors indicate sea surface temperature climatology (October–May 1980–2019; data: ERA5, Hersbach et al. 2020), and blue colors indicate winter-centered mean sea ice concentration (October–May 1980–2019; data: NSIDC, Cavalieri et al. 1996). The thick white line outlines the maximum winter sea ice extent for the year 2019. The three sections are the Barents Sea Opening (BSO) of Atlantic inflow hydrography and the northern gateway (NGW) and eastern gateway (EGW) of sea ice import.

accessibility to a changing Arctic. A better understanding of spatial sea ice variability and its drivers is therefore essential to realize sea ice predictions of societal relevance (Wagner et al. 2020). The predictive potential associated with the Atlantic inflow is probably the most explored (e.g., Schlichtholz 2011; Årthun et al. 2012; Nakanowatari et al. 2014; Schlichtholz 2019) and was already alluded to by Helland-Hansen and Nansen (1909). Onarheim et al. (2015) used the strong link between the Atlantic heat transport and sea ice area in Barents Sea—more heat, less sea ice—to predict skillfully the sea ice cover one year in advance. The predictability also extends to using inflow temperature instead of heat flux, overcoming the relative shortness of the current-meter measurements at BSO (Onarheim et al. 2015). However, the predictions only provide the aforementioned single areal number representing the whole domain, and accordingly little information about spatial variability. Predictive skill from sea ice import is less explored (Ellingsen et al. 2009), and the influence of the wind is generally understood to be immediate, which adds explanatory power but generally limits predictability (e.g., Onarheim et al. 2015).

Analysis of pan-Arctic sea ice concentration variability shows a spatial pattern that is characterized by an Atlantic

dipole with one center over the Barents and Greenland Seas and the other over the Labrador Sea, and one Pacific dipole with centers over the Sea of Okhotsk and the Bering Seas (e.g., Deser et al. 2000; Kauker et al. 2003; Koenigk et al. 2009; Close et al. 2017). A more detailed analysis, as presented here, of regional patterns of sea ice change and their underlying mechanisms has however not been performed. And although many studies have shed light on different mechanisms influencing a variable Barents Sea ice area (e.g., Sorteberg and Kvingedal 2006; Årthun et al. 2012; Pavlova et al. 2014; Lind et al. 2018; Docquier et al. 2020), the corresponding spatial patterns of sea ice retreat, expansion, and redistribution are relatively unknown.

Here, we provide a detailed study of the spatial variability of winter sea ice in the Barents Sea and identify the mechanisms associated with different spatial modes of interannual variability. The Barents Sea ice cover is strongly seasonal with essentially all ice melting in summer, and we therefore consider winter sea ice area (October–May) herein. We specifically assess the relative importance of inflow Atlantic Water hydrography, sea ice area import, regional winds, and surface heat loss in driving the identified spatial patterns of interannual sea ice variability. As outlined above, these mechanisms are a priori known to influence the Barents Sea ice area, but their spatiotemporal fingerprint has not yet been ascertained.

This paper is structured as follows. The datasets and methodology are presented in section 2. In section 3, we first outline the general trends and variability, and then identify the dominant modes of sea ice variability using an empirical orthogonal function analysis and establish the dominant drivers of each mode. The results are discussed in section 4, and a summary of the main conclusions is presented in section 5.

2. Data and methods

This paper investigates the dominant spatial patterns of sea ice variability in the Barents Sea and to what extent these patterns are associated with the inflow of Atlantic Water, sea ice import, regional winds, and surface heat flux. The Barents Sea is confined to the area between 13° and 63° E and 69° – 81° N (Fig. 1).

a. Sea ice concentration

We use monthly sea ice concentration (SIC), estimated from passive microwave satellite data from the National Snow and Ice Data Center (NSIDC) on a $25\text{ km} \times 25\text{ km}$ grid (Cavalieri et al. 1996) to obtain time series of sea ice concentration at each grid point and to summarize these into a total sea ice area (SIA) time series over the Barents Sea (Fig. 2). In each grid cell, we calculate winter sea ice concentration as an October–May mean to capture the whole season when sea ice is present, over the period 1980–2019. The indicated year denotes the winter-mean that ends in the respective year (e.g., 2019 represents October 2018–May 2019). Thereafter, we detrend the time series by removing the linear trend to focus on the interannual variability.

To assess the dominant spatiotemporal patterns of Barents Sea ice variability, we apply an empirical orthogonal function analysis (EOF; e.g., Zhang and Moore 2014). The analysis

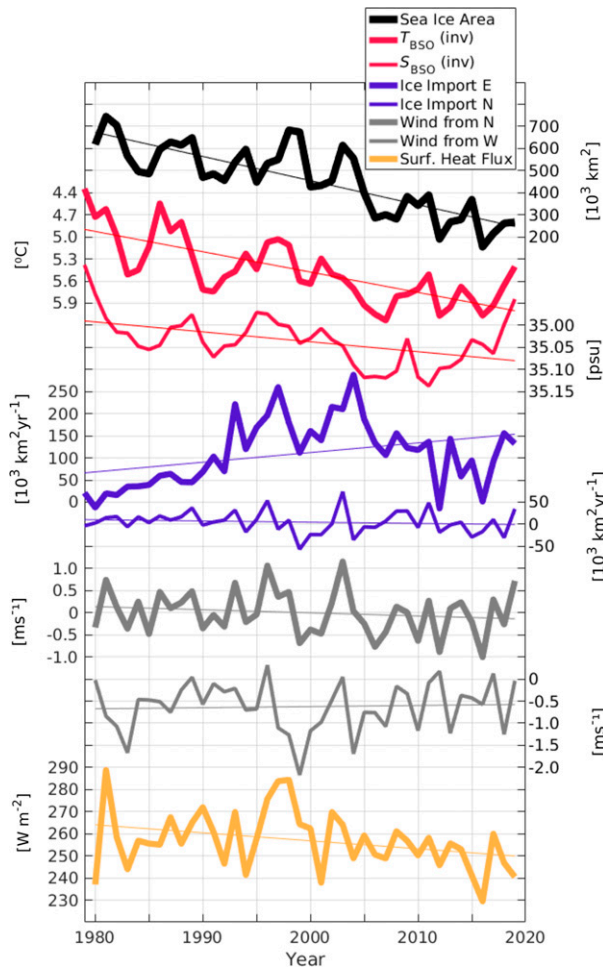


FIG. 2. Sea ice area and drivers of change. Barents Sea ice area (black line); Atlantic Water inflow temperature (thick red line) and salinity (thin red line) at the BSO; sea ice import through the eastern (EGW; blue thick line) and the northern (NGW; blue thin line) gateways; wind from the north (gray thick line) and wind from the west (gray thin line); and net surface heat flux (SHF; yellow line). Linear trends are plotted as thin solid lines. Note that the vertical axis of temperature and salinity are inverted. All time series are winter means (October–May) except AW hydrography that is winter-centered annual means (July–June).

sorts, in decreasing order of explained variance, the grid point time series into orthogonal pairs of spatial patterns (the EOFs) and their corresponding evolution in time, the principal component (PCs). The spatial patterns and their explained variance are not sensitive to using a shorter winter period (e.g., December–March).

b. Atlantic inflow at the Barents Sea Opening

To assess the influence of Atlantic Water inflow on the sea ice variability, we consider AW temperature (T_{BSO}) and salinity (S_{BSO}) at the Barents Sea Opening (BSO; 71.5°N, 20°E and 73.5°N, 20°E; Fig. 1) as provided via the ICES Report on Ocean Climate database (IROC; González-Pola et al. 2020),

where AW is defined as the water sampled between 50 and 200 m. This standard section has been sampled since 1977 by the Norwegian Institute of Marine Research (IMR), and is typically surveyed six times per year, thus capturing the seasonal cycle of the Atlantic inflow (Ingvaldsen et al. 2004).

As with sea ice, we detrend the time series for the period 1979–2019, although for AW temperature and salinity we use winter-centered annual mean (from July to the next June; Fig. 2), following, for example, Nakanowatari et al. (2014). Observations of volume and heat transport through the BSO are also available but only since 1998 (e.g., Skagseth et al. 2020). As the length of records is a critical constraint for the intercomparison of time series, including for the confidence in making inference, this study therefore assesses inflow influence using AW hydrography. We note that previous studies have found that sea ice area anomalies covary more with AW temperature than with volume transport (Årthun et al. 2012).

c. Sea ice import

Sea ice import is calculated for the straits between Novaya-Zemlya and Frans Josef Land [the eastern gateway (EGW): from 77°N, 67°E to 80.5°N, 62°E; Fig. 1] and between Svalbard and Frans Josef Land [the northern gateway (NGW): from 80.5°N, 27°E to 80.5°N, 45°E; Fig. 1] following Lind et al. (2018). The sea ice area inflow is calculated based on daily sea ice drift data a 25 km × 25 km grid from the NSIDC (Polar Pathfinder Daily 25-km EASE-Grid Sea Ice Motion Vectors, version 4; Tschudi et al. 2020).

Sea ice area import time series are calculated by following the procedure of Kwok (2009), using

$$F = \sum_{i=1}^{N-1} 0.5(u_i + u_{i+1})C_i\Delta x, \quad (1)$$

where u_i is the velocity component into the Barents Sea perpendicular to the passage, C_i is the sea ice concentration, and Δx is the distance in kilometers between each grid cell i in the passage, where N is the total number of grid cells. The EGW is aligned with the EASE-grid, whereas the NGW is not. For the latter case, we accordingly use trigonometric functions to calculate the velocity component perpendicular to the gateway in each grid cell across the gateway. Both time series are calculated as the winter-mean transport over October–May for the period 1979–2019, and afterward linearly detrended (Fig. 2).

d. Winds

To assess the impact of the atmospheric circulation on sea ice variability in the Barents Sea, we use monthly averaged data from ERA5 (Hersbach et al. 2020) of zonal and meridional 10-m wind and sea level pressure (SLP) on 0.25° × 0.25° grid resolution. We examine the direct impact of winds on sea ice by calculating the winter mean (October–May) zonal (u_{wind} ; positive eastward) and meridional (v_{wind} ; positive northward) components for the period 1980–2019 over the Barents Sea region (Fig. 2). To investigate whether the regional winds are influenced by large-scale atmospheric circulation we also examine the dominant SLP patterns for the Northern Hemisphere (30°–90°N) for the same period, identified from an EOF analysis.

e. Surface heat fluxes

We use surface latent, sensible, longwave, and shortwave heat fluxes from ERA5 (Hersbach et al. 2020) to estimate net surface heat fluxes (Fig. 2). Winter averages (October–May) are calculated for the ice-free southwestern Barents Sea (70°–74°N, 20°–30°E). The choice is somewhat arbitrary, but representative of open ocean conditions; the latter to represent the subsequent surface forcing of AW downstream of the BSO and to avoid the intermittency in heat loss related to the local presence of sea ice or not. Positive values are defined as upward (i.e., from the ocean to the atmosphere).

f. Correlation and regression

To assess the drivers of each spatial sea ice pattern (EOF) and its corresponding PC, we first apply standard lead–lag correlation and then linear regression analysis. Significant relationships are at the 95% confidence level unless otherwise stated, accounting for autocorrelation using the methods of Chelton (1983) for correlation and Ebisuzaki (1997) for regression related to gridded data. For the regression analysis, the predictor variables are the time series of Atlantic inflow hydrography (at the BSO), the ice import through the northern and eastern gateways, the averaged 10-m wind components over the Barents Sea domain, and the surface heat flux. The response variable is the anomalous sea ice concentration in the Barents Sea domain.

3. Results

Here we identify the spatial patterns of Barents Sea ice variability and their relationship with the known drivers of change alluded to above. We first provide an overview of the linear trends and anomalous variability in sea ice area and potential drivers (Fig. 2). Then we examine the dominant spatial patterns of interannual sea ice variability (Fig. 3), which is the main focus of this study, and we examine the impact of the drivers on each pattern (Figs. 4–6; Table 1). We specifically assess the relative roles of Atlantic inflow hydrography, sea ice import through the eastern and northern gateways (EGW and NGW), local winds, and surface heat flux.

a. Overview of the potential drivers

The general decrease in sea ice area over the satellite record is accompanied by warming and salinification of the Atlantic inflow, with long-term respective trends of about one (detrended) standard deviation per decade for sea ice and temperature, and half of that for salinity (Fig. 2; the standard deviations are $87 \times 10^3 \text{ km}^2$, 0.35°C , and 0.04 psu , respectively).

The sea ice area import is dominated by the eastern gateway. Its linear trend in is one of increase and it thus counteracts areal decrease. However, the import is also very much characterized by decadal variability. It increases over the first decades of the study and then, after 2004, the sea ice area import decreases; in extreme cases it even becomes negative (i.e., export in 2012).

The winter-mean (October–May) meridional wind varies interannually between southerly and northerly (Fig. 2, thick gray curve), with a slight trend toward more southerly wind (i.e., a mean wind increasingly contributes to keeping the Barents Sea ice free). However, the trend is not significant. The winter-mean zonal wind on the other hand, is in most years from the east (negative values), favoring sea ice import through the EGW (Fig. 2, thin gray curve).

The winter surface heat loss in the (ice-free) southern Barents Sea is large with a mean value of 258 W m^{-2} . It has nevertheless been decreasing over the time period considered, the linear trend being approximately 3.5 W m^{-2} per decade (Fig. 2, yellow curve; the standard deviation is 12 W m^{-2}).

Figure 2 and Table 1 show that the relation for trends and sea ice area carry over to interannual variability for all suggested drivers but sea ice import. Warmer and more saline inflow, stronger winds from the south, and anomalously low heat loss correspond to years of relatively less ice. As opposed to the case for trend, there is for interannual variability the intuitive relation that more sea ice area import (mainly from the east) increases the sea ice area of the Barents Sea. We note that the standard deviation of sea ice import ($82 \times 10^3 \text{ km}^2 \text{ yr}^{-1}$ for the total) is compatible with explaining the variable sea ice area alone, if these two were perfectly correlated.

Considering correlations, the potential drivers are statistically independent (covariance of 5% or less) except for the influence of the wind on the other drivers (summarized in Table 2) and the expected “spiciness” of inflow hydrography (warm anomalies tend to be saline; $r = 0.62$). Concerning the wind itself, also the zonal and meridional wind components are correlated (Table 2) as the dominant anomalous wind comes at an angle (southeast–northwest). We have, nevertheless, continued considering zonal and meridional winds for simplicity.

Regressing salinity on temperature, the anomalous inflow salinity can be separated into its covariance with temperature and one part independent of temperature. In doing so, we find all significant relations involving salinity herein to be explained by its covariance with temperature. The following assessments including AW inflow are therefore mainly concerned with temperature.

b. The dominant patterns of sea ice variability

We first document the dominant spatial patterns (EOFs) of sea ice variability in the Barents Sea and their associated temporal evolution (PCs) as outlined in section 2. The first three EOFs together explain 76% of the total variance in interannual sea ice concentration; they are found to be well separated, also from EOF4, following North’s rule of thumb (North et al. 1982; not shown).

The most dominant pattern (EOF1; Fig. 3a) explains 43% of the total winter sea ice area variance and displays a monopole spatial pattern with a center of action in the northeastern Barents Sea. In its positive phase (as shown in Fig. 3a), EOF1 is typically associated with sea ice concentration anomalies in the northeastern Barents Sea of about 15% per standard

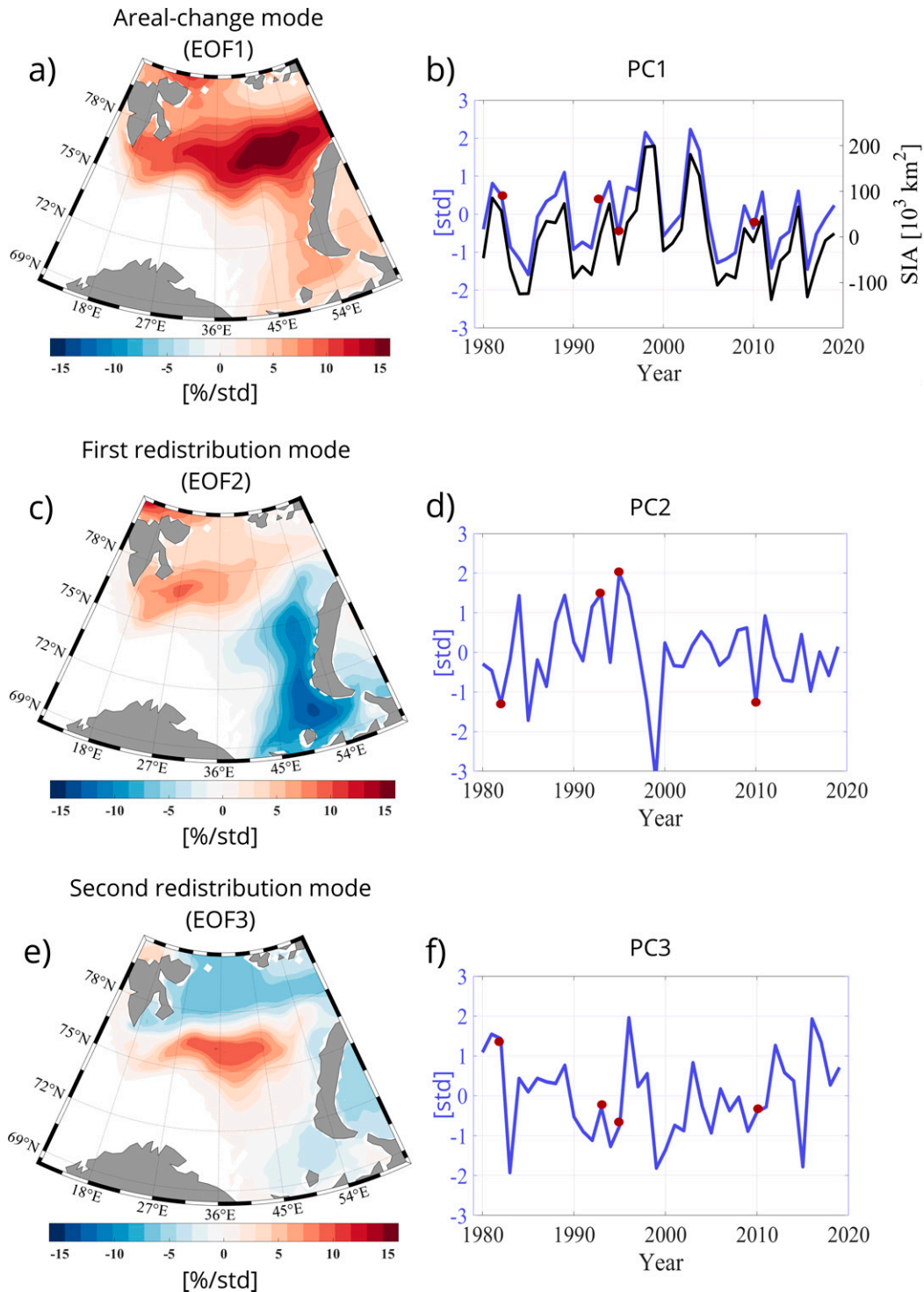


FIG. 3. The dominant patterns of Barents Sea ice concentration variability. The spatial modes (EOFs 1–3) are displayed in the left column, and their corresponding temporal evolution in the right (PCs 1–3, blue curves). The pairs explain 43%, 22%, and 11% of total variance, respectively. The color bars indicate anomalous sea ice concentration per standard deviation of the corresponding PC. The black curve is the temporal evolution of anomalous sea ice area (note the offset on the vertical axes). The red dots indicate years when either redistribution mode is relatively dominant.

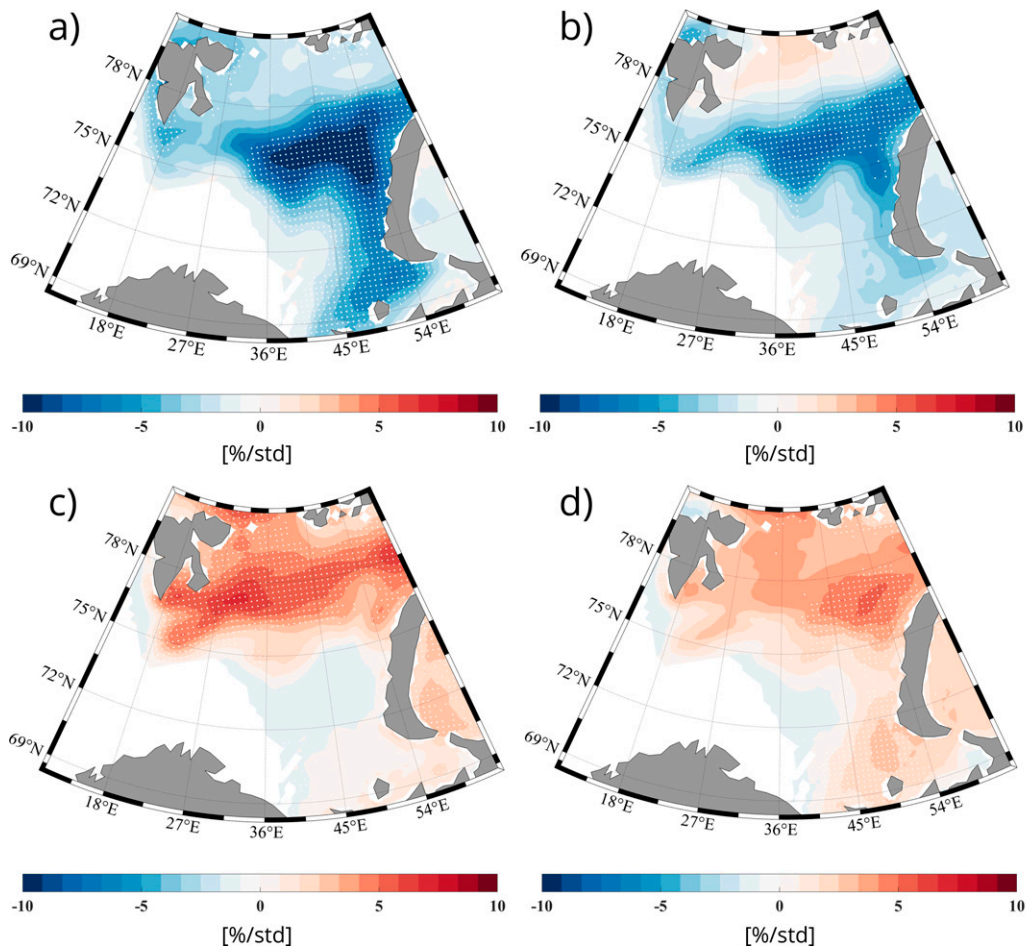


FIG. 4. Drivers of the areal-change mode. Regression of anomalous sea ice concentration on anomalous and standardized (a) BSO temperature (1-yr lag), (b) BSO salinity (1-yr lag), and (c),(d) eastern sea ice import (zero and 1-yr lag). White dots indicate significant regression values. The color bars indicate the predicted sea ice concentration anomaly per standard deviation of the predictor.

deviation of the corresponding PC. The most striking feature of its temporal evolution of the first EOF (PC1; Fig. 3b) is that it is for all practical purposes identical to the total sea ice area in the Barents Sea ($r = 0.99$; see Fig. 3b), and we will therefore refer to EOF1 as the *areal-change mode*.

The second pattern (EOF2; Fig. 3c) displays a dipolar structure and explains 22% of the total winter sea ice concentration variance. Specifically, in its positive phase (as shown in Fig. 3c), a positive sea ice anomaly southeast of Svalbard corresponds to a negative sea ice anomaly southwest of Novaya Zemlya. The magnitude of the sea ice concentration anomalies associated with EOF2 is generally smaller than for EOF1, with the exception in the region south of Novaya Zemlya.

Last, EOF3 (Fig. 3e; explaining 11% of the total winter sea ice variance) displays a tripole-like pattern with two of the centers of action in the central basin and in the northern Barents Sea, respectively, and an extended anomalous signal in the vicinity of Novaya Zemlya, but primarily on the Kara Sea side. As neither EOF2 nor EOF3 are concerned with changing the sea ice area (Table 1), we will refer to these modes as *redistribution modes*.

c. Drivers of sea ice variability

We now examine the mechanisms driving the identified the areal-change and redistribution modes of sea ice variability in the Barents Sea. For the areal-change mode, its temporal evolution being practically identical to that of anomalous sea ice area; the link with drivers is accordingly implied by the assessment of Fig. 2 above. We find that the variations in Atlantic Water temperatures in the BSO constitute a main driver of variability (Table 1). The response in sea ice extent lags temperature changes by one year, consistent with the time needed for Atlantic Water from BSO to reach the ice edge (Smedsrud et al. 2010; Årthun et al. 2012). In further support of AW inflow as a major driver of the areal-change mode, we find that the spatial footprint that appears when regressing sea ice concentration on AW hydrography (Figs. 4a,b) is very similar to that of the areal-change mode (EOF1; Fig. 3a).

The areal-change mode (EOF1) is also significantly influenced by sea ice import from the Arctic Ocean (Table 1). For

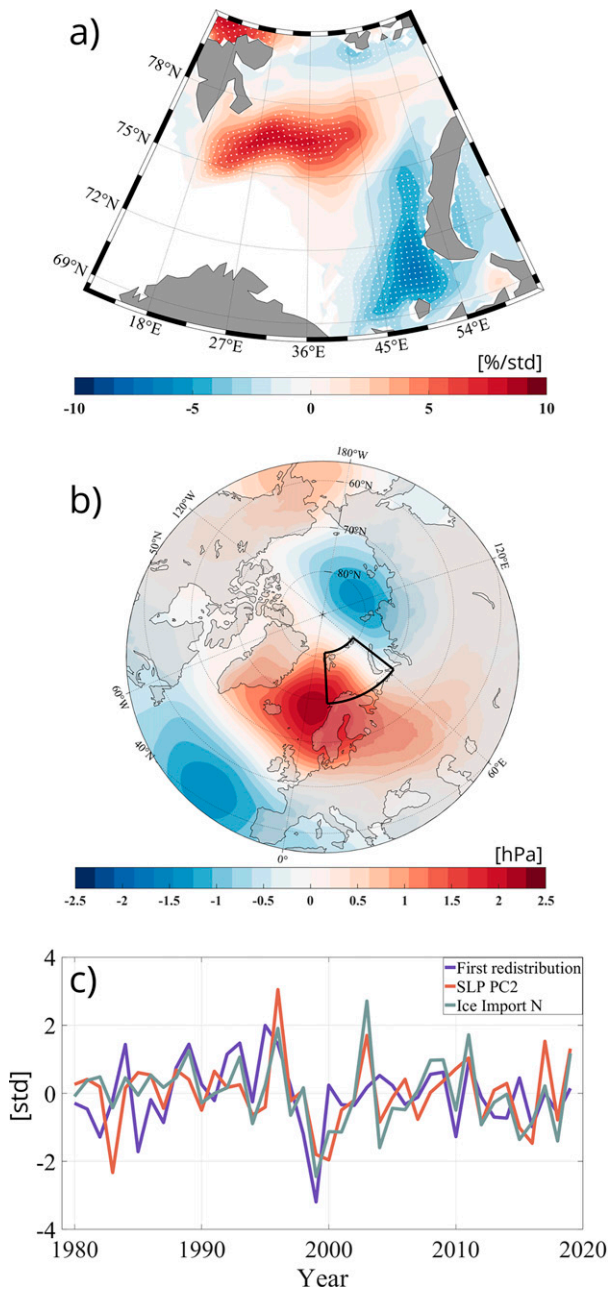


FIG. 5. Drivers of the first redistribution mode (EOF2). (a) Regression of anomalous sea ice concentration on anomalous and standardized northern sea ice import (zero lag). White dots indicate significant regression values. The color bar indicates the predicted sea ice concentration anomaly per standard deviation of the northern sea ice import. (b) Second EOF of sea level pressure (SLP) for the Northern Hemisphere (30°–90°N; October–May; explains 12% of total SLP variance). (c) The corresponding principal component (SLP-PC2; red line), the first redistribution mode (blue line; from Fig. 3d), and northern sea ice import (light green line).

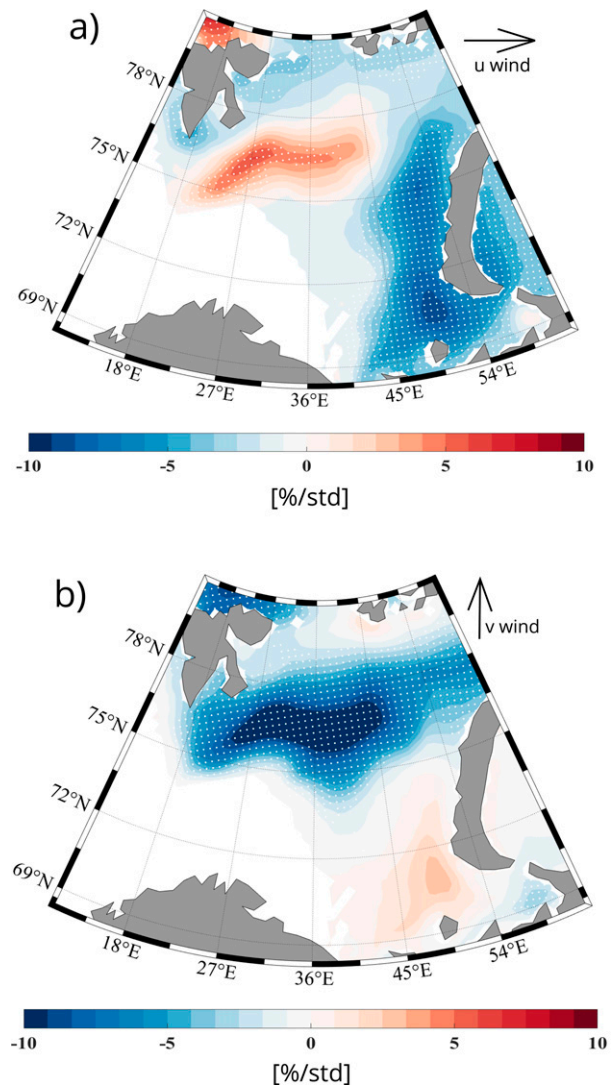


FIG. 6. Barents Sea ice concentration response to wind. Regression of anomalous sea ice concentration on anomalous and standardized (a) zonal and (b) meridional winds. White dots indicate significant regression values. The color bar indicates the predicted sea ice concentration anomaly per standard deviation of the respective wind component.

the eastern gateway (EGW; F_E), there is a direct relationship between the sea ice import and the sea ice area ($r = 0.44$). The eastern sea ice import impacts the sea ice cover mainly in a zonal belt in the northern Barents Sea (Fig. 4c). We note that Atlantic Water temperature and the eastern ice import are not significantly correlated, implying that these are two independent mechanisms that influence the areal change of Barents Sea ice.

Before reaching the sea ice, ocean temperature anomalies are also influenced by substantial atmosphere–ocean interaction (Schlichtholz and Houssais 2011; Skagseth et al. 2020). This is reflected in the correlation between surface heat fluxes and PC1 ($r = 0.41$; Table 1), that is, less surface

TABLE 1. Correlations of anomalous sea ice area (SIA) and the PCs of the dominant spatial patterns (EOFs) of sea ice concentration with the main drivers: Atlantic Water temperature (T_{BSO}) and salinity (S_{BSO}), eastern (F_E) and northern (F_N) ice area import, average 10-m wind components (u_{wind} and v_{wind}), and net surface heat fluxes (SHF). All the variables are calculated as winter means (October–May) except AW hydrography, which uses winter-centered annual means (July–June). The notation @year indicates lead time (@1 is 1-yr lead time). Bold (bold italic) indicates significance at the 95% (90%) confidence level according to Chelton (1983).

	SIA	$T_{\text{BSO}}(@1)$	$S_{\text{BSO}}(@1)$	F_E	F_N	u_{wind}	v_{wind}	SHF(@1)	SHF
SIA	1	-0.51	-0.31	0.44	0.05	-0.29	-0.48	0.47	0.41
PC1	0.98	-0.51	-0.34	0.48	0.15	-0.17	-0.56	0.42	0.41
PC2	-0.18	0.23	0.13	0.26	0.50	0.54	-0.40	-0.40	0.04
PC3	-0.07	-0.25	-0.32	-0.27	0.43	0.42	-0.36	-0.18	0.16

heat loss corresponding to reduced sea ice area. There is also a similar correlation when surface heat fluxes lead by one year ($r = 0.42$).

Sea ice import through the northern gateway (NGW; F_N) and local winds are important drivers for the redistribution modes (EOF2 and EOF3) and their temporal variability (Table 1). We find that the local wind significantly impacts the sea ice area import to the Barents Sea (Table 2) and the temporal variability of all the three leading modes of sea ice concentration in the Barents Sea (PCs 1–3; Table 1). This finding supports that the sea ice import to the Barents Sea is predominantly wind-driven, in line with, for example, Kwok et al. (2013). Persistent zonal winds from the east (Fig. 2, thin gray curve) give a stable sea ice inflow to the Barents Sea through the EGW (Fig. 2, blue thick curve). The meridional wind component has a strong impact on the interannual variability of sea ice import particularly through the NGW (Fig. 2, thin blue curve; Table 2).

The spatial footprint of northern ice import (regressed on anomalous sea ice concentration; Fig. 5a) and zonal winds (Fig. 6a) are both similar to that of the first redistribution mode (EOF2; Fig. 3c). The spatial footprint of meridional winds (Fig. 6b) has a broad center of action at the central Barents Sea that encloses the central core of the second redistribution mode (EOF3; Fig. 3e).

The redistribution modes are also related to the surface heat flux within the Barents Sea. For PC2 there is a significant correlation when surface heat flux leads by 1 year ($r = -0.42$). The regression pattern of surface heat fluxes onto SIC the following winter also resembles EOF2, and especially the eastern center of action (Figs. 3c and 7b).

TABLE 2. Correlations between the zonal and meridional wind (u_{wind} and v_{wind} , positive from west to east and from south to north, respectively) and Atlantic water temperature (T_{BSO}), eastern (F_E) and northern (F_N) sea ice import, net surface heat fluxes (SHF), and sea level pressure second principal component (SLP-PC2) without lag. All the variables are calculated as winter means (October–May) except AW temperature that is winter-centered annual mean (July–June). Bold indicates significance at the 95% confidence level according to Chelton (1983).

	T_{BSO}	F_E	F_N	u_{wind}	v_{wind}	SHF	SLP-PC2
u_{wind}	-0.05	-0.20	0.67	1	-0.37	0.01	0.61
v_{wind}	0.47	-0.34	-0.74	-0.37	1	-0.56	-0.73

4. Discussion

The winter sea ice cover of the Barents Sea displays large fluctuations superimposed on the long-term loss. Here we have identified the spatial patterns characteristic of this interannual variability (Fig. 3). The temporal evolution (PC1) of the dominant spatial pattern (EOF1) is essentially identical to that of anomalous sea ice area (Figs. 3a,b). We accordingly name EOF1 the “areal-change mode.” We note that a similar relation has previously been pointed out in passing by Schlichtholz (2019), but not investigated in detail. We find that this near-identical correspondence between the leading EOF and the most frequently used “metric” for sea ice change is both very useful and in need of explanation.

Our suggestion is that the (almost) perfect correlation arises for two reasons. First, the larger the coherent change in sea ice concentration across the domain, the larger the net change in mean concentration for the Barents Sea and thus its sea ice area (the linear measure, or metric, of mean concentration is nevertheless different from the quadratic metric of total covariance. The latter is what is maximized in the procedure of singular value decomposition used to identify the EOFs and corresponding PCs). Second, the sea ice edge (or, rather, the sea ice concentration of the marginal ice zone) is generally interconnected and fluctuates as a large-scale feature (i.e., coherently, and thus to change the area).

EOF analysis decomposes the variance of gridded time series data into independent (orthogonal) statistical modes. With the variance of net areal change in essence being perfectly represented by the leading EOF, all the remaining modes (EOFs) and corresponding time series (PCs) thus only contribute—individually and combined—to redistribute the sea ice (without changing the total area of sea ice cover). These are accordingly “redistribution modes.” While the areal-change mode is dominant in explaining total variance (EOF1 explains 43% whereas EOF2 and EOF3 explain 22% and 11% respectively), redistribution in total explains 57%. The sea ice fluctuation is thus more about redistribution than changing the area covered (the long-term trend aside). Redistribution accordingly dominates the sea ice variability in the Barents Sea in certain years. For example, during the years 1982, 1993, 1995, and 2010, when the amplitude of the areal-change PC1 is small ($PC1 \leq 0.5$), the amplitude of one or both of the redistribution modes PC2 and PC3 is larger than

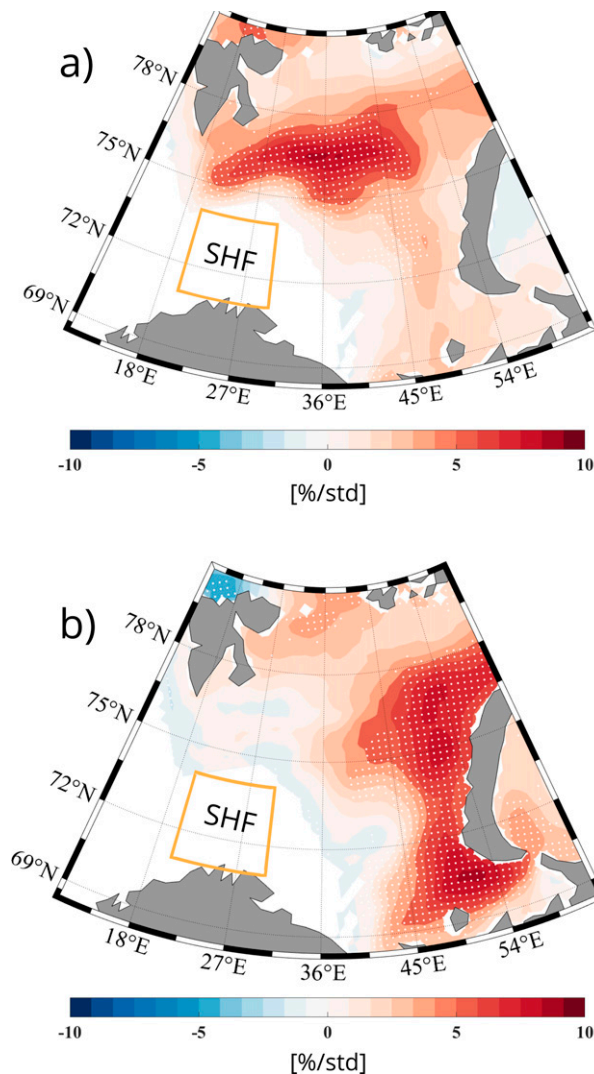


FIG. 7. Barents Sea ice concentration response to surface heat flux. Regression of anomalous sea ice concentration on (a) anomalous and standardized surface heat fluxes, and when (b) the surface heat flux leads by one year. The yellow box indicates the area the heat fluxes are averaged over. White dots indicate significant regression values. The color bar indicates the predicted sea ice concentration anomaly per standard deviation of the surface heat flux.

one standard deviation (Figs. 3b,d,f). During the winter 1993, when PC2 dominates, the pattern of sea ice concentration anomaly was similar to EOF2 (not shown). During the winter 1995, when both PC2 and PC3 dominate, the sea ice concentration pattern (not shown) is similar to the EOF2 dipole pattern, but also with a negative minimum at the central Barents Sea—a result of the significant contribution of PC3.

a. Areal-change mode

The pattern of the areal-change mode in the Barents Sea shows that most of this variability occurs in the central and

northeastern part of Barents Sea (Fig. 3a). This pattern is very similar to the spatial pattern of the linear trend in sea ice concentration (see Fig. 1 in Onarheim and Årthun 2017), in line with the relationships carrying over from interannual variability to trend (Fig. 2). The spatial pattern of the areal change mode furthermore closely resembles that identified from the analysis of pan-Arctic winter sea ice concentration variability (Deser et al. 2000; Kauker et al. 2003; Koenigk et al. 2009; Close et al. 2017). This highlights the importance of the Barents Sea in recent changes in Arctic winter sea ice, in line with previous studies (e.g., Onarheim et al. 2018).

The importance of the Atlantic inflow in maintaining the ice-free area of the Barents Sea is well established from previous studies (e.g., Helland-Hansen and Nansen 1909; Årthun et al. 2012; Herbaut et al. 2015). This includes downstream “Atlantification,” the expansion of the Atlantic Water domain outlining the sea ice retreat (Årthun et al. 2012). Kauker et al. (2003) also found the leading pattern of Arctic winter sea ice concentration variability to reflect anomalous ocean heat transport through the BSO. Anomalous AW salinity is also related to a variable sea ice cover (Table 1; Fig. 4b), but, as previously mentioned, this relation is rooted in the covariance between salinity and temperature, both being a manifestation of a variable Atlantic inflow.

Our study also shows that surface heat fluxes and sea ice import between Novaya Zemlya and Franz Josef Land (EGW) are important for changing the sea ice area. At zero lag, the impact of these drivers is closely connected to regional winds, evident by their significant correlations with meridional winds (Table 2). Specifically, anomalous northerly winds will lead to more sea ice in the Barents Sea both by transporting more sea ice into the region (Kwok 2009) and by increasing surface heat loss (Schlichtholz and Houssais 2011).

There is also a significant correlation between the areal change mode (PC1) and surface heat fluxes when heat fluxes lead by one year (Table 1). This delayed response is consistent with the reemergence mechanism described by, for example, Schlichtholz and Houssais (2011) and Bushuk et al. (2019), in which anomalous surface heat loss in winter and spring is an important driver of ocean temperature anomalies, and thus sea ice area, the following winter.

The eastern ice import also has a 1-yr delayed effect. This delayed response is suggestive of sea ice melt during summer influencing the upper-ocean stratification, and hence making the conditions more favorable for sea ice production the following winter since a stronger stratification reduces vertical mixing and heat fluxes from the deep Atlantic Water below the halocline (Rudels 1987; Lind et al. 2016, 2018). There is also a substantial 1-yr autocorrelation, ($r = 0.61$), for the eastern sea ice area import, suggesting that there is an overall memory of the (external) sea ice conditions from one year to the next in addition to the direct influence on the import from the wind.

Our analysis has focused on interannual variability. Considering the general sea ice decrease over the satellite record, a warming of the Atlantic inflow has generally accompanied it. Reduced surface heat loss shows that the Atlantic Water is also being less cooled during its passage

through the Barents Sea (Fig. 2; Skagseth et al. 2020). Taking the long-term (linear) trend into account, a warming of the Atlantic Water inflow can explain most of the sea ice loss (Fig. 2). The dominant role of ocean temperature on long-term sea ice change and the importance of ice import on interannual time scales are consistent with the identified drivers of sea ice variability and retreat north of Svalbard (Onarheim et al. 2014).

b. Redistribution modes

The second and third modes of sea ice variability in the Barents Sea (Figs. 3c,e) do not impact the total sea ice area, and are thus referred to as “redistribution” modes. The temporal variability and spatial pattern of the first redistribution mode (EOF2) can be explained by variable ice import between Svalbard and Franz Josef Land (NGW), local winds over the Barents Sea (Table 1; Fig. 5a), and surface heat fluxes (Table 1; Fig. 7b). Variability in these different drivers is closely connected. For example, northerly winds lead to increased ice import to the northern Barents Sea (Kwok 2009; Herbaut et al. 2015) but also to reduced ice growth along Novaya Zemlya as a result of less heat loss (Moore 2013) and less polynya activity (Martin and Cavalieri 1989). This contrasting geographical response is responsible for the dipole pattern between the northwestern and southeastern Barents Sea that characterizes EOF2. The import of sea ice through the NGW is smaller and more variable, but can be substantial in some years, in which case it has significant impact on the Barents Sea ice concentration (Kwok et al. 2005; Aaboe et al. 2021).

The second sea ice redistribution mode (EOF3) is associated with meridional winds. The regression (zero lag) of sea ice concentration on meridional winds (Fig. 6b) encloses the dominant center of action of the second redistribution mode (Fig. 3c). The pattern furthermore resembles that obtained from the regression of sea ice variability onto the Atlantic Water temperature at BSO at no lag found by Herbaut et al. (2015). In our analysis we also find significant correlations between meridional wind and Atlantic Water temperature at zero lag ($r = 0.47$; Table 2). We thus interpret this pattern as a result of wind-driven changes in Atlantic Water heat transport that affect the sea ice concentration immediately (Lien et al. 2017). EOF3 also shows a lagged response to surface heat fluxes two years prior. A detailed investigation of this 2-yr lag is not presented here. We note, however, that 2 years is equal to the flushing time (i.e., the memory of the Barents Sea; Smedsrud et al. 2010) and we therefore suggest that the abovementioned mechanism also applies here.

c. Large-scale forcing of sea ice import

Our results confirm that sea ice import is an important driver of Barents Sea ice variability, in line with previous studies (e.g., Kwok et al. 2005; Kwok 2009; Ellingsen et al. 2009; Koenig et al. 2009; Lind et al. 2018). The sea ice import in turn shows strong links with local wind variations (Table 2; Kwok 2009). To examine the association between the large-scale atmospheric circulation, we perform an EOF

analysis of the winter (October–May) sea level pressure (SLP) over the Northern Hemisphere (north of 30°N). The first mode of SLP variability is the Arctic Oscillation (AO; explaining 54% of the variability). The AO is significantly related to zonal winds over the Barents Sea ($r = -0.49$) but not to meridional winds (not shown). The second pattern of SLP variability (explaining 12% of the total variability) has an anticyclonic circulation over Norwegian Sea and a cyclonic circulation over Kara Sea, causing northwesterly winds over Barents Sea (Fig. 5b). The corresponding temporal evolution (SLP-PC2; Fig. 5c) is associated with both the local winds and the northern sea ice import (NGW) to Barents Sea (Fig. 5c, Table 2), and, as a consequence, with the first redistribution mode (SIC-PC2; Fig. 5c). Note that SLP-PC2 in particular captures the large sea ice export (import) in 1999 (2003) (Fig. 5c). In contrast, we find no significant correlation between EGW ice import and any of the two first leading modes of SLP variability at zero lag.

Several previous studies have investigated the dominant patterns of atmospheric circulation in the Arctic region (e.g., Wu et al. 2006; Overland and Wang 2010; Alexeev et al. 2017). The patterns however differ somewhat depending on the domain, dataset, and period considered, making a direct comparison to Fig. 5b difficult. Previous studies have also focused mainly on the Arctic Oscillation/North Atlantic Oscillation and their influence on anomalous sea ice transport through the Fram Strait, and not into the Barents Sea (e.g., Wu et al. 2006; Kwok 2009; Kwok et al. 2013). Finally, it is worth mentioning that it has not been previously established that the sea ice inflow from the NGW and the EGW are independent ($r = 0.04$) and thus different atmospheric circulations are forcing the sea ice flow through the two gateways

5. Conclusions

In this study we have identified the characteristic spatial patterns of interannual sea ice variability in the Barents Sea and their associated relation to known drivers of sea ice change using observational and reanalysis data from 1979 to 2019. Potential predictability is particularly associated with the dominant mode because of its lagged response to Atlantic inflow, sea ice import, and surface heat fluxes. The other modes, related to the redistribution of the sea ice concentration (without changing the area), appear relatively unpredictable (unless the drivers themselves can be predicted). Sea ice is redistributed as a direct response (zero lag) to sea ice import, wind, and surface heat fluxes.

The dominant spatial pattern of sea ice variability is the fluctuating marginal ice zone, with its largest imprint on the central and northeastern Barents Sea generally corresponding to the pathway of Atlantic Water upon facing the ice (EOF1; Figs. 2a,b). It explains 43% of the total interannual spatial variance in sea ice concentration and is for all practical purposes identical to the change in sea ice area (Schlichtholz 2019). We therefore term this mode the “areal-change mode” of the variable Barents Sea ice cover.

The pattern amplifies, and thus sea ice area increases with more sea ice import from the east, northerly winds, the lagged response (one year) to colder inflow of Atlantic Water and more ocean heat loss. There is also a lagged response (one year) to sea ice import from the east (between Franz Josef Land and Novaya Zemlya; EGW). First, there is the tendency that one high-import year is followed by another ($r = 0.57$). Autocorrelation aside, we interpret more sea ice import to leave a more stratified ocean locally over summer, reducing vertical mixing with the deep layer of Atlantic Water and accommodating more local freezing in the following winter. In addition, larger sea ice inflow means there will be more sea ice to melt, and thus less surface water warming in the summer (Lind et al. 2018), also favoring sea ice production in the following winter (Screen and Simmonds 2010).

The direct predictive potential to the areal-change mode thus relates to the lagged response to Atlantic inflow and sea ice import, but the two drivers impact in different areas of the Barents Sea. The Atlantic inflow impacts primarily in the central and northeastern Barents Sea, whereas the sea ice inflow through the EGW impacts in an east–west belt in the northern Barents Sea (Fig. 4). These predictors for sea ice area, as a scalar quantity, are well known (e.g., Sorteberg and Kvingedal 2006; Årthun et al. 2012; Pavlova et al. 2014; Onarheim et al. 2015; Wang et al. 2019; Schlichtholz 2019).

The remaining modes of variability do not impact the total sea ice area and redistribute sea ice within the Barents Sea, primarily due to the influence of the wind, and we accordingly term these “redistribution modes” (predominantly EOF2 and EOF3, explaining 20% and 11% of the variance, respectively; Figs. 3c–f). EOF2 is mainly driven by the ice import from the north (between Svalbard and Franz Josef Land; NGW), which in turn is associated with large-scale sea level pressure changes, and by the lagged response to anomalous surface heat fluxes in the southern Barents Sea. EOF3 mainly responds to meridional winds, which force a direct response in the Atlantic throughflow (Herbaut et al. 2015; Lien et al. 2017). The contribution of anomalous sea ice import in itself can intuitively be associated with changing the spatial distribution of sea ice downstream but also with a net change in area. The import’s key role in explaining the redistribution modes thus takes place in a combination with other drivers, including local melting and freezing, so that the total area is conserved (including that the import that does change area is reflected in its correlation with the areal-change mode).

Our results expand on previous work on the area-integrated sea ice variability in the Barents Sea (e.g., Årthun et al. 2012; Pavlova et al. 2014; Onarheim et al. 2015) by identifying the spatial footprint associated with this “areal change” and further with the independent footprints of “redistribution.” By disentangling the spatial patterns of the relatively predictable areal-change mode from the more unpredictable redistribution modes, our study also improves the understanding of interannual sea ice variability in the Barents Sea and the causes thereof. The spatial patterns and mechanisms of variability identified herein thus provide observation-based benchmarks for understanding the spatial nature of sea ice change, and for assessing skill—including its cause and effect—in dynamical

prediction models and in ice-ocean or coupled climate models in general.

Acknowledgments. This study was funded by the Research Council of Norway projects PATHWAY (Grant 263223), Seasonal Forecasting Engine (Grant 270733), and Nansen Legacy (Grant 276730), the Blue-Action project (European Union’s Horizon 2020 research and innovation program; Grant 727852), and the Trond Mohn Foundation (Grant BFS2018TMT01).

Data availability statement. All data used in this study are freely available. Sea ice concentration data are available at <https://nsidc.org/data/nsidc-0051> and sea ice velocities at <https://nsidc.org/data/NSIDC-0116/versions/4>. Time series of temperature and salinity are available from <https://ocean.ices.dk/core/iroc>. Surface heat fluxes, 10-m wind components, and sea level pressure from ERA5 are available at <https://cds.climate.copernicus.eu/cdsapp#!/dataset/reanalysis-era5-single-levels-monthly-means?tab=form>. The analysis carried out in this paper is based on standard Matlab functions except for the Ebisuzaki function we use to estimate significant regression values, which is available at <https://se.mathworks.com/matlabcentral/fileexchange/10881-weaclim>.

REFERENCES

- Aaboe, E., S. Lind, S. Hendricks, E. Down, T. Lavergne, and R. Ricker, 2021: Sea-ice and ocean conditions surprisingly “normal” in Svalbard-Barents Sea region after large sea-ice inflows in 2019: Copernicus Marine Service Ocean State Report (issue 5). *J. Operational Oceanogr.*, **14** (Suppl. 1), 1–185, <https://doi.org/10.1080/1755876X.2021.1946240>.
- Alexeev, V. A., J. E. Walsh, V. V. Ivanov, V. A. Semenov, and A. V. Smirnov, 2017: Warming in the Nordic seas, North Atlantic storms and thinning Arctic sea ice. *Environ. Res. Lett.*, **12**, 084011, <https://doi.org/10.1088/1748-9326/aa7a1d>.
- Årthun, M., T. Eldevik, L. Smedsrud, Ø. Skagseth, and R. Ingvaldsen, 2012: Quantifying the influence of Atlantic heat on Barents Sea ice variability and retreat. *J. Climate*, **25**, 4736–4743, <https://doi.org/10.1175/JCLI-D-11-00466.1>.
- , I. H. Onarheim, J. Dörr, and T. Eldevik, 2021: The seasonal and regional transition to an ice-free Arctic. *Geophys. Res. Lett.*, **48**, e2020GL090825, <https://doi.org/10.1029/2020GL090825>.
- Bushuk, M., X. Yang, M. Winton, R. Msadek, M. Harrison, A. Rosati, and R. Gudgel, 2019: The value of sustained ocean observations for sea ice predictions in the Barents Sea. *J. Climate*, **32**, 7017–7035, <https://doi.org/10.1175/JCLI-D-19-0179.1>.
- Carmack, E., and Coauthors, 2015: Toward quantifying the increasing role of oceanic heat in sea ice loss in the new Arctic. *Bull. Amer. Meteor. Soc.*, **96**, 2079–2105, <https://doi.org/10.1175/BAMS-D-13-00177.1>.
- Cavalieri, D., and Coauthors, 1996: Sea ice concentrations from Nimbus-7 SMMR and DMSP SSM/I-SSMIS passive microwave data, version 1 (updated yearly). NASA National Snow and Ice Data Center Distributed Active Archive Center, accessed April 2021, <https://doi.org/10.5067/8GQ8LZQVL0VL>.
- Chelton, D. B., 1983: Effects of sampling errors in statistical estimation. *Deep-Sea Res.*, **30A**, 1083–1103, [https://doi.org/10.1016/0198-0149\(83\)90062-6](https://doi.org/10.1016/0198-0149(83)90062-6).

- Close, S., M.-N. Houssais, and C. Herbaut, 2017: The Arctic winter sea ice quadrupole revisited. *J. Climate*, **30**, 3157–3167, <https://doi.org/10.1175/JCLI-D-16-0506.1>.
- Deser, C., J. E. Walsh, and M. S. Timlin, 2000: Arctic sea ice variability in the context of recent atmospheric circulation trends. *J. Climate*, **13**, 617–633, [https://doi.org/10.1175/1520-0442\(2000\)013<0617:ASIVIT>2.0.CO;2](https://doi.org/10.1175/1520-0442(2000)013<0617:ASIVIT>2.0.CO;2).
- Docquier, D., R. Fuentes-Franco, T. Koenigk, and T. Fichefet, 2020: Sea ice–ocean interactions in the Barents Sea modeled at different resolutions. *Front. Earth Sci.*, **8**, 172, <https://doi.org/10.3389/feart.2020.00172>.
- Ebisuzaki, W., 1997: A method to estimate the statistical significance of a correlation when the data are serially correlated. *J. Climate*, **10**, 2147–2153, [https://doi.org/10.1175/1520-0442\(1997\)010<2147:AMTETS>2.0.CO;2](https://doi.org/10.1175/1520-0442(1997)010<2147:AMTETS>2.0.CO;2).
- Ellingsen, I., D. Slagstad, and A. Sundfjord, 2009: Modification of water masses in the Barents Sea and its coupling to ice dynamics: A model study. *Ocean Dyn.*, **59**, 1095–1108, <https://doi.org/10.1007/s10236-009-0230-5>.
- González-Pola, C., K. Larsen, P. Fratantoni, and A. Beszczynska-Moller, 2020: ICES report on ocean climate 2019. ICES Cooperative Research Rep. 350, 136 pp., <https://doi.org/10.17895/ices.pub.7537>.
- Helland-Hansen, B., and F. Nansen, 1909: *The Norwegian Sea: Its Physical Oceanography Based upon the Norwegian Researches 1900–1904*. Det Mallingske Bogtrykkeri, 360 pp.
- Herbaut, C., M.-N. Houssais, S. Close, and A.-C. Blaizot, 2015: Two wind-driven modes of winter sea ice variability in the Barents Sea. *Deep-Sea Res. I*, **106**, 97–115, <https://doi.org/10.1016/j.dsr.2015.10.005>.
- Hersbach, H., and Coauthors, 2020: The ERA5 global reanalysis. *Quart. J. Roy. Meteor. Soc.*, **146**, 1999–2049, <https://doi.org/10.1002/qj.3803>.
- Ingvaldsen, R. B., L. Asplin, and H. Loeng, 2004: Velocity field of the western entrance to the Barents Sea. *J. Geophys. Res.*, **109**, C03021, <https://doi.org/10.1029/2003JC001811>.
- Kauker, F., R. Gerdes, M. Karcher, C. Köberle, and J. L. Lieser, 2003: Variability of Arctic and North Atlantic sea ice: A combined analysis of model results and observations from 1978 to 2001. *J. Geophys. Res.*, **108**, 3182, <https://doi.org/10.1029/2002JC001573>.
- Koenigk, T., U. Mikolajewicz, J. H. Jungclaus, and A. Kroll, 2009: Sea ice in the Barents Sea: Seasonal to interannual variability and climate feedbacks in a global coupled model. *Climate Dyn.*, **32**, 1119–1138, <https://doi.org/10.1007/s00382-008-0450-2>.
- Kwok, R., 2009: Outflow of Arctic Ocean sea ice into the Greenland and Barents Seas: 1979–2007. *J. Climate*, **22**, 2438–2457, <https://doi.org/10.1175/2008JCLI2819.1>.
- , W. Maslowski, and S. W. Laxon, 2005: On large outflows of Arctic sea ice into the Barents Sea. *Geophys. Res. Lett.*, **32**, L22503, <https://doi.org/10.1029/2005GL024485>.
- , G. Spreen, and S. Pang, 2013: Arctic sea ice circulation and drift speed: Decadal trends and ocean currents. *J. Geophys. Res. Oceans*, **118**, 2408–2425, <https://doi.org/10.1002/jgrc.20191>.
- Lien, V. S., P. Schlichtholz, Ø. Skagseth, and F. B. Vikebø, 2017: Wind-driven Atlantic water flow as a direct mode for reduced Barents Sea ice cover. *J. Climate*, **30**, 803–812, <https://doi.org/10.1175/JCLI-D-16-0025.1>.
- Lind, S., R. B. Ingvaldsen, and T. Furevik, 2016: Arctic layer salinity controls heat loss from deep Atlantic layer in seasonally ice-covered areas of the Barents Sea. *Geophys. Res. Lett.*, **43**, 5233–5242, <https://doi.org/10.1002/2016GL068421>.
- , —, and —, 2018: Arctic warming hotspot in the northern Barents Sea linked to declining sea-ice import. *Nat. Climate Change*, **8**, 634–639, <https://doi.org/10.1038/s41558-018-0205-y>.
- Martin, S., and D. J. Cavalieri, 1989: Contributions of the Siberian shelf polynyas to the Arctic Ocean intermediate and deep water. *J. Geophys. Res.*, **94**, 12 725–12 738, <https://doi.org/10.1029/JC094iC09p12725>.
- Moore, G., 2013: The Novaya Zemlya Bora and its impact on Barents Sea air–sea interaction. *Geophys. Res. Lett.*, **40**, 3462–3467, <https://doi.org/10.1002/grl.50641>.
- Nakanowatari, T., K. Sato, and J. Inoue, 2014: Predictability of the Barents Sea ice in early winter: Remote effects of oceanic and atmospheric thermal conditions from the North Atlantic. *J. Climate*, **27**, 8884–8901, <https://doi.org/10.1175/JCLI-D-14-00125.1>.
- North, G. R., T. L. Bell, R. F. Cahalan, and F. J. Moeng, 1982: Sampling errors in the estimation of empirical orthogonal functions. *Mon. Wea. Rev.*, **110**, 699–706, [https://doi.org/10.1175/1520-0493\(1982\)110<0699:SEITEO>2.0.CO;2](https://doi.org/10.1175/1520-0493(1982)110<0699:SEITEO>2.0.CO;2).
- Onarheim, I. H., and M. Årthun, 2017: Toward an ice-free Barents Sea. *Geophys. Res. Lett.*, **44**, 8387–8395, <https://doi.org/10.1002/2017GL074304>.
- , L. H. Smedsrud, R. B. Ingvaldsen, and F. Nilsen, 2014: Loss of sea ice during winter north of Svalbard. *Tellus*, **66A**, 23933, <https://doi.org/10.3402/tellusa.v66.23933>.
- , T. Eldevik, M. Årthun, R. B. Ingvaldsen, and L. H. Smedsrud, 2015: Skillful prediction of Barents Sea ice cover. *Geophys. Res. Lett.*, **42**, 5364–5371, <https://doi.org/10.1002/2015GL064359>.
- , —, L. H. Smedsrud, and J. C. Stroeve, 2018: Seasonal and regional manifestation of Arctic sea ice loss. *J. Climate*, **31**, 4917–4932, <https://doi.org/10.1175/JCLI-D-17-0427.1>.
- Overland, J. E., and M. Wang, 2010: Large-scale atmospheric circulation changes are associated with the recent loss of Arctic sea ice. *Tellus*, **62A** (1), 1–9, <https://doi.org/10.1111/j.1600-0870.2009.00421.x>.
- Pavlova, O., V. Pavlov, and S. Gerland, 2014: The impact of winds and sea surface temperatures on the Barents Sea ice extent, a statistical approach. *J. Mar. Syst.*, **130**, 248–255, <https://doi.org/10.1016/j.jmarsys.2013.02.011>.
- Rudels, B., 1987: *On the Mass Balance of the Polar Ocean, with Special Emphasis on the Fram Strait*. Norsk Polarinstittutt, 188 pp.
- , E. P. Jones, U. Schauer, and P. Eriksson, 2004: Atlantic sources of the Arctic Ocean surface and halocline waters. *Polar Res.*, **23**, 181–208, <https://doi.org/10.1111/j.1751-8369.2004.tb00007.x>.
- Schlichtholz, P., 2011: Influence of oceanic heat variability on sea ice anomalies in the Nordic Seas. *Geophys. Res. Lett.*, **38**, L05705, <https://doi.org/10.1029/2010GL045894>.
- , 2019: Subsurface ocean flywheel of coupled climate variability in the Barents Sea hotspot of global warming. *Sci. Rep.*, **9**, 13692, <https://doi.org/10.1038/s41598-019-49965-6>.
- , and M.-N. Houssais, 2011: Forcing of oceanic heat anomalies by air–sea interactions in the Nordic seas area. *J. Geophys. Res.*, **116**, C01006, <https://doi.org/10.1029/2009JC005944>.
- Screen, J. A., and I. Simmonds, 2010: The central role of diminishing sea ice in recent Arctic temperature amplification. *Nature*, **464**, 1334–1337, <https://doi.org/10.1038/nature09051>.

- , and —, 2013: Exploring links between Arctic amplification and mid-latitude weather. *Geophys. Res. Lett.*, **40**, 959–964, <https://doi.org/10.1002/grl.50174>.
- Skagseth, Ø., T. Eldevik, M. Årthun, H. Asbjørnsen, V. S. Lien, and L. H. Smedsrud, 2020: Reduced efficiency of the Barents Sea cooling machine. *Nat. Climate Change*, **10**, 661–666, <https://doi.org/10.1038/s41558-020-0772-6>.
- Smedsrud, L. H., R. Ingvaldsen, J. E. Ø. Nilsen, and Ø. Skagseth, 2010: Heat in the Barents Sea: Transport, storage, and surface fluxes. *Ocean Sci.*, **6**, 219–234, <https://doi.org/10.5194/os-6-219-2010>.
- , and Coauthors, 2013: The role of the Barents Sea in the Arctic climate system. *Rev. Geophys.*, **51**, 415–449, <https://doi.org/10.1002/rog.20017>.
- Sorokina, S. A., C. Li, J. J. Wettstein, and N. G. Kvamstø, 2016: Observed atmospheric coupling between Barents Sea ice and the warm-Arctic cold-Siberian anomaly pattern. *J. Climate*, **29**, 495–511, <https://doi.org/10.1175/JCLI-D-15-0046.1>.
- Sorteberg, A., and B. Kvingedal, 2006: Atmospheric forcing on the Barents Sea winter ice extent. *J. Climate*, **19**, 4772–4784, <https://doi.org/10.1175/JCLI3885.1>.
- Spren, G., R. Kwok, and D. Menemenlis, 2011: Trends in Arctic sea ice drift and role of wind forcing: 1992–2009. *Geophys. Res. Lett.*, **38**, L19501, <https://doi.org/10.1029/2011GL048970>.
- Tschudi, M. A., W. N. Meier, and J. S. Stewart, 2020: An enhancement to sea ice motion and age products at the National Snow and Ice Data Center (NSIDC). *Cryosphere*, **14**, 1519–1536, <https://doi.org/10.5194/tc-14-1519-2020>.
- Wagner, P. M., and Coauthors, 2020: Sea-ice information and forecast needs for industry maritime stakeholders. *Polar Geogr.*, **43**, 160–187, <https://doi.org/10.1080/1088937X.2020.1766592>.
- Wang, Q., and Coauthors, 2019: Ocean heat transport into the Barents Sea: Distinct controls on the upward trend and interannual variability. *Geophys. Res. Lett.*, **46**, 13 180–13 190, <https://doi.org/10.1029/2019GL083837>.
- Woods, C., and R. Caballero, 2016: The role of moist intrusions in winter Arctic warming and sea ice decline. *J. Climate*, **29**, 4473–4485, <https://doi.org/10.1175/JCLI-D-15-0773.1>.
- Wu, B., and M. A. Johnson, 2007: A seesaw structure in SLP anomalies between the Beaufort Sea and the Barents Sea. *Geophys. Res. Lett.*, **34**, L05811, <https://doi.org/10.1029/2006GL028333>.
- , J. Wang, and J. E. Walsh, 2006: Dipole anomaly in the winter Arctic atmosphere and its association with sea ice motion. *J. Climate*, **19**, 210–225, <https://doi.org/10.1175/JCLI3619.1>.
- Zhang, Z., and J. C. Moore, 2014: *Mathematical and Physical Fundamentals of Climate Change*. Elsevier, 494 pp.